British Journal of Pharmacology (2005) 146, 445–455
www.nature.com/bjp

Mechanisms of xenon- and isoflurane-induced preconditioning – a potential link to the cytoskeleton *via* the MAPKAPK-2/HSP27 pathway

*,[1]Nina C. Weber, [1]Octavian Toma, [1]Jessica I. Wolter, [1]Nicole M. Wirthle, [1]Wolfgang Schlack & [1]Benedikt Preckel

[1]Department of Anesthesiology, University Hospital of Düsseldorf, Moorenstrasse 5, 40225 Düsseldorf, Germany

1 We previously demonstrated that the anesthetic gas xenon exerts cardioprotection by preconditioning *in vivo via* activation of protein kinase C (PKC)-ε and p38 mitogen-activated protein kinase (MAPK). P38 MAPK interacts with the actin cytoskeleton *via* the MAPK-activated protein kinase-2 (MAPKAPK-2) and heat-shock protein 27 (HSP27). The present study further elucidated the underlying molecular mechanism of xenon-induced preconditioning (Xe-PC) by focusing on a potential link of xenon to the cytoskeleton.

2 Anesthetized rats received either xenon (Xe-PC, $n=6$) or the volatile anesthetic isoflurane (Iso-PC, $n=6$) during three 5-min periods interspersed with two 5-min and one final 10-min washout period. Control rats ($n=6$) remained untreated for 45 min. Additional rats were either pretreated with the PKC inhibitor Calphostin C (0.1 mg kg^{-1}) or with the p38 MAPK inhibitor SB203580 (1 mg kg^{-1}) with and without anesthetic preconditioning (each, $n=6$). Hearts were excised for immunohistochemistry of F-actin fibers and phosphorylated HSP27. Phosphorylation of MAPKAPK-2 and HSP27 were assessed by Western blot. HSP27 and actin colocalization were investigated by co-immunoprecipitation.

3 Xe-PC induced phosphorylation of MAPKAPK-2 (control 1.0 ± 0.2 vs Xe-PC 1.6 ± 0.1, $P<0.05$) and HSP27 (control 5.0 ± 0.5 vs Xe-PC 9.8 ± 1.0, $P<0.001$). Both effects were blocked by Calphostin C and SB203580. Xe-PC enhanced translocation of HSP27 to the particulate fraction and increased F-actin polymerization. F-actin and pHSP27 were colocalized after Xe-PC.

4 Xe-PC activates MAPKAPK-2 and HSP27 downstream of PKC and p38 MAPK. These data link Xe-PC to the cytoskeleton, revealing new insights into the mechanisms of Xe-PC *in vivo*.
British Journal of Pharmacology (2005) **146,** 445–455. doi:10.1038/sj.bjp.0706324;
published online 8 August 2005

Keywords: Xenon; cardiac preconditioning; cytoskeleton; F-actin fibers; heat-shock protein 27; MAPKAPK-2

Abbreviations: CC, Calphostin C; DMSO, dimethyl sulfoxide; HSP27, heat-shock protein 27; Iso, isoflurane; MAPK, mitogen-activated protein kinase; MAPKAPK-2, MAPK activated protein kinase-2; PKC, protein kinase C; Xe-PC, xenon preconditioning

Introduction

In the last years *volatile* anesthetics, that are halogenated fluorocarbons like isoflurane, have been increasingly recognized to mimic the strong cardioprotection against ischemia reperfusion damage exerted by *ischemic* preconditioning (IPC) (Cason *et al*., 1997). This phenomenon, known as *pharmacological* preconditioning induced by anesthetics (*anesthetic* preconditioning), has been described *in vitro* and *in vivo* (Mullenheim *et al*., 2002; 2003), but to date it is completely unknown which final end-effector mediates the cardioprotection induced by anesthetics. Moreover, the single steps of the signalling cascade of anesthetic-induced preconditioning remain to be elucidated.

We could recently demonstrate that the 'chemically' inert *gas* xenon, a gas with anesthetic properties, induces pharmacological preconditioning in the rat heart *in vivo* to the same extent as IPC does. In the case of pharmacological preconditioning by xenon, this cardioprotective effect was mediated *via* protein kinase C (PKC)-ε and its downstream target p38 mitogen-activated protein kinase (MAPK) (Weber *et al*., 2005). Since xenon is used as an anesthetic gas with minimal hemodynamic and cardiovascular side effects (Schmidt *et al*., 2001; Preckel *et al*., 2002b) in comparison with the more pronounced hemodynamic effects of the volatile anesthetics (Preckel *et al*., 2002a; Rossaint *et al*., 2003), this inert gas might become an ideal anesthetic for patients with a high-risk for perioperative cardiac events.

The present study aimed to further elucidate the underlying molecular mechanism of xenon-induced preconditioning (Xe-PC) in comparison with preconditioning by the volatile anesthetic isoflurane.

Based on our previous findings of the functional involvement of p38 MAPK (Weber *et al*., 2005), we focused on two important downstream targets of p38 MAPK, the MAPK-activated protein kinase 2 (MAPKAPK-2) and the small heat-shock protein 27 (HSP27). An influence of xenon on these both enzymes would link Xe-PC to the actin cytoskeleton of the myocardial cell and provide substantial new information

*Author for correspondence; E-mail: Nina.Weber@uni-duesseldorf.de

about the signal transduction pathway towards the *end*-effector of xenon-induced cardioprotection.

In response to diverse physiological and pathological stimuli, p38 MAPK is rapidly activated in the heart (Clerk *et al*., 1998; Haq *et al*., 1998; Magne *et al*., 2001) and it plays an important role in ischemia reperfusion injury (Abe *et al*., 2000). P38 MAPK affects the phosphorylation of HSP27 (Gaestel *et al*., 1991) *via* the MAPKAPK-2. Phosphorylation of HSP27 results in the translocation of this enzyme to the actin filaments of the cell network. Thus, HSP27 is an important regulator of actin polymerization (Miron *et al*., 1991). Unphosphorylated HSP27 inhibits the actin polymerization by depolymerization of the actin filaments. This depolymerization is mediated by the binding of monomers or small oligomers of HSP27 to the barbed end of the filament (Benndorf *et al*., 1994). In consequence, G-actin monomers are no longer able to be incorporated into the filament and the F-actin polymerization is inhibited. Besides this *inhibitory* property of HSP27 on the actin polymerization process, phosphorylation of HSP27 has been shown to enhance its cytoprotective activity by stabilizing the actin cytoskeleton (Guay *et al*., 1997).

Based on our recent results, it is of special interest that HSP27 has also been described to be directly related with the PKC signal transduction pathway (Bitar, 2002). However, to date, there exist no data addressing the exact molecular mechanism of preconditioning induced by the inert gas xenon. Therefore, the results of the present study give important information about potential downstream targets of PKC and p38 MAPK and may contribute to elucidate the cellular mechanism of xenon-induced pharmacological preconditioning.

Methods

The study was performed in accordance with the regulations of the German Animal Protection Law and was approved by the Bioethics Committee of the District of Düsseldorf. Male Wistar rats ((200–250 g), 6 per group) were anesthetized by intraperitoneal *S*-ketamine injection (150 mg kg^{-1}). *S*-ketamine does not interfere with preconditioning (Mullenheim *et al*., 2001) and an effect of *S*-ketamine on the investigated enzymes was excluded by additional Western blot analyses comparing animals with *S*-ketamine and without (killed by cervical dislocation) *S*-ketamine treatment (data not shown). Animals had free access to food and water at all times before the start of the experiments.

Materials

Xenon was kindly provided by Messer Griessheim GmbH (Krefeld, Germany). Calphostin C, SB203580, Protein-G-Agarose immunoprecipitation kit, rabbit polyclonal anti-actin antibody and monoclonal α-tubulin mouse antibody were purchased from Sigma (Taufkirchen, Germany). The enhanced chemiluminescence protein detection kit was purchased from Santa Cruz (Heidelberg, Germany). Phospho MAPKAPK-2 and total MAPKAPK-2 rabbit polyclonal antibodies were from Cell Signalling (Frankfurt/M, Germany) as was the p38 MAPK assay kit. Phospho HSP27 rabbit polyclonal antibody was from Dianova (Hamburg, Germany) and total HSP25 (the rodent homologue of HSP27) rabbit polyclonal antibody was from Stressgen Biotechnology (Victoria, Canada). Peroxidase-conjugated goat anti-rabbit and donkey anti-mouse antibodies were from Jackson Immunolab (Dianova, Hamburg, Germany). Rhodamine phalloidin and Alexa Fluor® 488 goat anti-rabbit antibody were from Molecular Probes (Göttingen, Germany). All other materials were either purchased from Sigma (Taufkirchen, Germany) or Merck-Eurolab (Munich, Germany).

Experimental protocol

Rats were divided into nine groups (Figure 1).

Control group (n = 6): After surgical preparation rats received 25% oxygen plus 75% nitrogen three times 5-min before the hearts were excised (total baseline 45 min).

Xenon-preconditioned group (Xe-PC) (n = 6): Rats received xenon 70% (equivalent to 0.43 minimal alveolar concentration (MAC) in rats) for three 5-min periods, interspersed with two 5-min wash-out periods 10 min before excision of the hearts (total treatment phase 35 + 10 min baseline = 45 min before the hearts were excised). The other 30% gas consisted of 5% nitrogen and 25% oxygen.

Isoflurane-preconditioned group (Iso-PC) (n = 6): Rats received an equianesthetic concentration of isoflurane (0.6 vol%, corresponding to 0.43 MAC isoflurane in rats (Rampil *et al*., 2001)) before excision of the hearts (total treatment phase 35 + 10 min baseline = 45 min before the hearts were excised). The remaining gas consisted of 75% nitrogen and 25% oxygen.

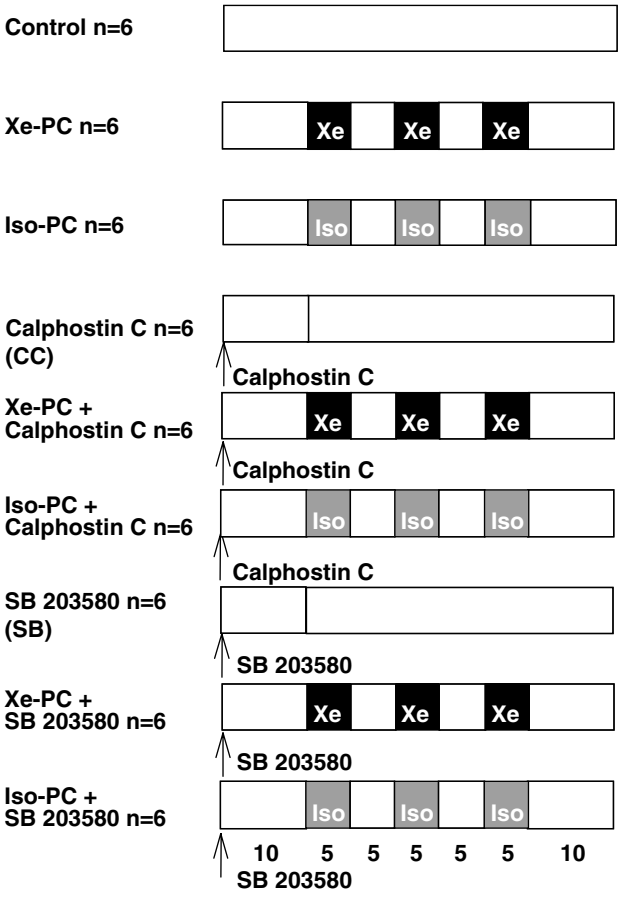

Figure 1 Experimental protocol: Xe = xenon, Iso = isoflurane, PC = preconditioning, SB = SB203580.

Control with Calphostin C group (n=6): Calphostin C (0.1 mg kg^{-1} in DMSO 1% aqueous solution) was intravenously administered 45 min before the hearts were excised.

Xenon + Calphostin C group (n=6): Xenon-preconditioned rats received Calphostin C (0.1 mg kg^{-1}) intravenously 10 min before xenon administration (total treatment phase: 35 + 10 min preinfusion of inhibitor = 45 min before the hearts were excised).

Isoflurane + Calphostin C group (n=6): Isoflurane-preconditioned rats intravenously received Calphostin C (0.1 mg kg^{-1}) 10 min before isoflurane administration (total treatment phase: 35 + 10 min preinfusion of inhibitor = 45 min before the hearts were excised).

Control with SB203580 group (n=6): SB203580 (1 mg kg^{-1} in DMSO 1% aqueous solution) was intravenously administered 45 min before excision of the hearts.

Xenon + SB203580 group (n=6): Xenon-preconditioned rats received SB203580 (1 mg kg^{-1}) intravenously 10 min before xenon administration (total treatment phase: 35 + 10 min preinfusion of inhibitor = 45 min before the hearts were excised).

Isoflurane + SB203580 group (n=6): Isoflurane-preconditioned rats intravenously received SB203580 (1 mg kg^{-1}) 10 min before isoflurane administration (total treatment phase: 35 + 10 min preinfusion of inhibitor = 45 min before the hearts were excised).

In preliminary experiments we excluded an effect of DMSO alone on activation of the respective kinase in Western blot (data not shown).

Surgical preparation

Further preparation was performed as described previously (Weber *et al*., 2005). In brief, the male Wistar rats (200–250 g) were anesthetized by intraperitoneal *S*-ketamine injection (150 mg kg^{-1}). All animals were left untreated for 10 min before the start of the respective preconditioning protocol. In summary, after tracheal intubation, the lungs were ventilated with oxygen-enriched air and a positive end-expiratory pressure of 2–3 cm H_2O. Respiratory rate was adjusted to maintain PCO_2 within physiological limits. Body temperature was maintained at 38°C by the use of a heating pad. The right jugular vein was cannulated for saline and drug infusion, and the left carotid artery was cannulated for measurement of aortic pressure. Anesthesia was maintained by continuous α-chloralose infusion. A lateral left-sided thoracotomy followed by pericardiotomy was performed and a ligature (5–0 prolene) was passed below the main branch of the left coronary artery. After completion of the baseline time (see above) the hearts were excised and shock frozen immediately. Arterial blood gases were analyzed at baseline and kept within physiological ranges. Aortic pressure and electrocardiographic signals were digitized using an analog to digital converter (PowerLab/8SP, ADInstruments Pty Ltd, Castle Hill, Australia) at a sampling rate of 500 Hz and were continuously recorded on a personal computer using Chart for Windows v5.0 (ADInstruments Pty Ltd, Castle Hill, Australia).

Separation of particulate and cytosolic fraction

For cellular fractionation and subsequent Western blot assay of MAPKAPK-2 and HSP27, tissue specimens were prepared for protein analysis or immunohistochemistry to investigate HSP27 activation and distribution (particulate-, cytosolic fraction) within the myocytes. The excised hearts were frozen in liquid nitrogen. Subsequently, a cellular fractionation was performed that was adapted from the literature (Kang *et al*., 1999; Mackay & Mochly-Rosen, 2001; Chen *et al*., 2003). This technique allows separating the tissue into different fractions containing different cellular constituents. The frozen tissue was pulverized and dissolved in lysis buffer containing Tris base, EGTA, NaF and Na_3VO_4 (as phosphatase inhibitors), a freshly added protease inhibitor mix (aprotinin, leupeptin and pepstatin), 100 μM ml^{-1} okadaeic-acid and DTT. The solution was vigorously homogenized on ice (Homogenisator, IKA) and then centrifuged at 1000 × *g*, 4°C, for 10 min. This centrifugation at low speed allows a raw separation between the cytosolic fraction that still contains cellular organelles and their membranes and the particulate fraction containing myofibrils. The supernatant, containing cytosolic fraction, was centrifuged again at 16,000 × *g*, 4°C, for 15 min to clean up this fraction and to separate the mitochondria and other cellular organelles from this fraction. The remaining pellet was resuspended in lysis buffer containing 1% Triton X-100, incubated for 60 min on ice and vortexed. The solution was centrifuged at 16,000 × *g*, 4°C, for 15 min. The pellet containing the particulate fraction was collected and dissolved in lysis buffer for further Western blot assays.

Western blot analysis

After protein determination by the Lowry method (Lowry *et al*., 1951), equal amounts of protein were mixed with loading buffer (1 : 1) containing Tris-HCl, glycerol and bromphenol blue. Samples were vortexed and boiled at 95°C before being subjected to SDS–PAGE. Samples were loaded on a 10% SDS electrophoresis gel. The proteins were separated by electrophoresis and transferred onto a PVDF membrane by tank blotting (100 V, 1 h). Unspecific binding of the antibody was blocked by incubation with 5% fat dry milk powder or bovine serum albumin solution in Tris-buffered saline containing Tween (TBS-T) for 2 h. Subsequently, the membrane was incubated overnight at 4°C with the respective primary antibody at indicated concentrations. After washing in fresh, cold TBS-T, the blot was subjected to the appropriate horseradish peroxidase conjugated secondary antibody for 2 h at room temperature. Immunoreactive bands were visualized by chemiluminescence detected on X-ray film (Hyperfilm ECL, Amersham) using the enhanced chemiluminescence system of Santa Cruz. The blots were quantified using a Kodak Image station® (Eastman Kodak Comp., Rochester, NY, U.S.A.) and the results are presented as ratio of phosphorylated protein to total protein after multiplication of the average light intensity by 10 to facilitate the presentation of an *x*-fold increase. Equal loading of protein was additionally proved by detection of α-tubulin.

Co-immunoprecipitation of Actin and HSP27

Both enzymes were co-immunoprecipitated using the protein-G-agarose kit of Sigma. After protein determination by the method of Lowry *et al*. (1951), the samples (particulate fraction) were diluted to a concentration of 1 mg ml^{-1} up to a total volume of 200 μl. Actin in these samples was

immunoprecipitated by using a rabbit polyclonal anti-actin antibody in a special spin column overnight at 4°C. During this overnight incubation, the agarose beads were prepared as described by the supplier of the co-immunoprecipitation kit (Sigma). Before starting the experiment, 30 μl of the beads were washed twice with 1 ml of cold 1 × immunoprecipitation buffer (supplied by Sigma) by gentle vortexing and spinning in a microcentrifuge at 12,000 × *g* for 30 s. The supernatant was removed and 50 μl fresh cold immunoprecipitation buffer was added to the protein agarose and this protein agarose bead suspension was used for the subsequent co-immunoprecipitation. The agarose beads were transferred to the incubation mix of antibody and cell lysate. The resulting solution was again incubated overnight mixing the tube by inversion. The next day, samples were microcentrifuged for 15–30 s at 12,000 × *g*. The remaining pellets were washed five times with immunoprecipitation buffer containing EGTA, NaF and Na_3VO_4 (as phosphatase inhibitors) and a freshly added protease inhibitor mix (aprotinin, leupeptin and pepstatin). The final pellet was resuspended in 100 μl lysis buffer (see above), boiled at 95°C for 5 min, centrifuged again at 12,000 × *g* for 2 min and processed further by Western blot analysis detecting actin and phosphorylated HSP27 in order to evaluate the protein/protein interactions.

p38 MAPK activity assay

To investigate the activity of p38 MAPK, a nonradioactive p38 MAPK activity assay kit (Cell Signalling) was used. We investigated the enzyme activity of p38 MAPK after treatment with either xenon or isoflurane in order to confirm our recent results of an increased phosphorylation of p38 MAPK after xenon and isoflurane treatment. In this assay, the p38 MAPK downstream target ATF-2 is detected after its phosphorylation by the *active* p38 MAPK in the presence of ATP.

After protein determination by the method of Lowry *et al*. (1951), the samples were diluted to a concentration of 1 mg ml^{-1} up to a total volume of 200 μl. The active/phosphorylated p38 MAPK of these samples was immunoprecipitated by an immobilized anti-phospho-p38 antibody overnight at 4°C. The next day, samples were microcentrifuged for 1 min at 18,000 × *g*. The remaining pellets were washed twice with lysis buffer containing EDTA, EGTA, Triton-X, Na_3VO_4 and Leupeptin and with kinase buffer containing β-glycerolphosphate, DTT, Na_3VO_4 and $MgCl_2$. In the following, the pellets were resuspended in 50 μl kinase buffer supplemented with ATP (200 μM) and ATF-2 fusion protein (2 μg) and incubated for 30 min at 30°C. The reaction was stopped by addition of 3 × SDS sample buffer containing Tris-HCl, SDS, Glycerol, DTT and bromphenol blue.

The samples were boiled at 95°C for 5 min, centrifuged again at 18,000 × *g* for 2 min and processed further by Western blot analysis as described above. The membranes were incubated first with anti-phospho-ATF-2 antibody and second with a total ATF-2 antibody at indicated concentrations.

Immunohistochemistry

A cryo-microtome (Leica, Wetzlar, Germany) was used to obtain thin 5 μm sections from hearts that were placed and processed on microscopic slides (Superfrost®, Medite Medizintechnik, Burgdorf, Germany). One half of two control, xenon- and isoflurane-treated hearts was cut. The sections were air dried and fixed in Zamboni solution (4% paraformaldehyde, 15% picric acid), briefly washed in phosphate-buffered saline solution (PBS) and unspecific binding was blocked with 10% goat serum for 2 h at room temperature. After two further washing steps with PBS, slides were incubated with an appropriate concentration of rhodamine phalloidin (1 : 100) for 30 min at 4°C in the dark. Rhodamine phalloidin was removed by two further washing steps and the cuts were incubated with a rabbit anti-phospho-HSP27 (1 : 100) antibody for 1 h at room temperature. After washing with PBS, the slices were incubated with a goat anti-rabbit Alexa Fluor® 488 conjugated secondary antibody (1 : 200) for 1 h at room temperature in the dark. The stained sections were embedded and visualized using a fluorescence microscope (Leica-DML, Wetzlar, Germany) (Rhodamine phalloidin: excitation: 554 nm; emission: 573 nm, and Alexa Fluor: excitation: 497 nm; emission: 519 nm), original magnification: × 630.

Statistical analysis

Data are expressed as means ± s.e.m. Group comparisons were analyzed by a one-way ANOVA (Graph Pad Prism version 3.00) followed by Bonferroni's correction for multiple comparisons. Values with $^{*}P<0.05$ were considered statistically significant vs control group. Values with $^{\dagger}P<0.05$ were considered statistically significant vs Xe-PC group. Values with $^{\ddagger}P<0.05$ were considered statistically significant vs Iso-PC group.

Results

Direct measurement of p38 MAPK activity

Xenon led to a marked phosphorylation of ATF-2 compared with controls (12.2 ± 2.5 vs 3.2 ± 0.9, $P<0.05$, Figure 2). Changes in phosphorylation of ATF-2 were not caused by different amounts of ATF-2, as demonstrated by a uniform distribution of total ATF-2 (Figure 2 lower Western blot). Isoflurane also increased the phosphorylation of ATF-2 to 11.5 ± 3.0 ($P<0.05$ vs controls, Figure 2). Since we could previously show that myocardial protection was completely blocked by the use of the specific PKC inhibitor Calphostin C (Weber *et al*., 2005), we investigated if Calphostin C blocks the increased activity of p38 MAPK. In fact, Calphostin C abolished the effect of xenon and isoflurane on ATF-2 phosphorylation (4.5 ± 1.2 and 4.1 ± 0.5, $P<0.05$ vs xenon or isoflurane PC, respectively, Figure 2). Calphostin C alone had no significant effect on ATF-2 phosphorylation (4.3 ± 0.9, $P>0.05$ vs control, Figure 2).

Regulation of MAPKAPK-2 phosphorylation

The most important downstream target linking p38 MAPK to the cytoskeleton is MAPKAPK-2. The phosphorylation of MAPKAPK-2 was significantly increased both after xenon and isoflurane administration (1.6 ± 0.1 and 1.5 ± 0.1 vs 1.0 ± 0.1 in controls, $P<0.01$ and <0.05, respectively, Figure 3). The changes in phosphorylation of MAPKAPK-2 were expressed as a ratio of pMAPKAPK-2 to total MAPKAPK-2 (Figure 3, lower Western blot). The blockade

of PKC and p38 MAPK by Calphostin C and SB203580 abolished these effects (Figure 3), suggesting MAPKAPK-2 to be located downstream of both enzymes in the signalling cascade. The inhibitors alone had no effect on MAPKAPK-2 phosphorylation (1.1 ± 0.1 and 1.2 ± 0.1, both $P > 0.05$ vs control, Figure 3).

Phosphorylation of small heat-shock protein HSP27

Additionally, we aimed to clarify whether Xe-PC can induce the activation and translocation of the small heat-shock protein HSP27, which plays an important role in the reorganization of the actin cytoskeleton network of the cell. Both, xenon and isoflurane increased the phosphorylation of HSP27 compared to controls (9.7 ± 1.0 and 9.6. ± 0.9 vs 5.0 ± 0.4 in controls, both $P < 0.001$, respectively, Figure 4a). In order to calculate the ratio of phosphorylation of HSP27 to total HSP27 protein, total HSP27 was detected on the blot (Figure 4a, middle Western blot). Uniformity of protein distribution on the respective Western blot was confirmed by detection of α-tubulin (Figure 4a, lower Western blot). Calphostin C and SB203580 abolished the increased phosphorylation Figure 4a. The blockers itself had no effect on HSP27 phosphorylation (4.0 ± 0.3 and 4.7 ± 0.5, both $P > 0.05$ vs control, Figure 4a).

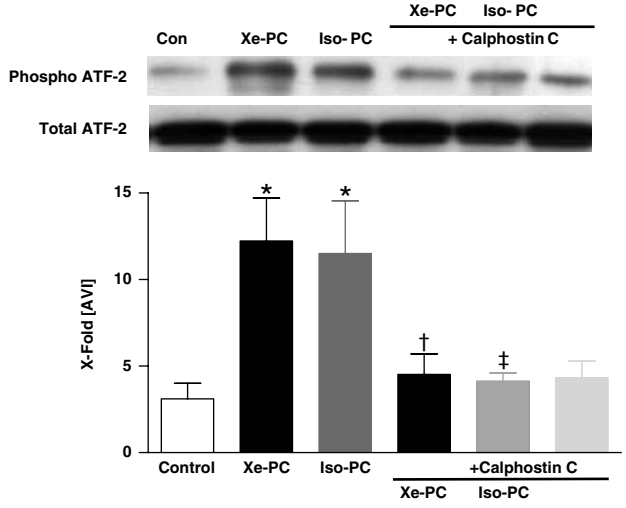

Figure 2 Activity assay of p38 MAPK. One representative Western blot experiment after immunoprecipitation of active p38 MAPK and incubation with ATP of cytosolic fraction of control and xenon- or isoflurane-treated hearts in the presence or absence of Calphostin C and SB203580 (each $n = 6$) is shown. Upper panel shows phosphorylated form of ATF-2, and lower panel total ATF-2. The histogram presents densitometric evaluation as *x*-fold average light intensity (AVI). Data show ratio of phosphorylated vs total ATF-2 (means ± s.e.m.). $^{*}P < 0.05$ vs control, $^{\dagger}P < 0.05$ vs Xe-PC and $^{\ddagger}P < 0.05$ vs Iso-PC.

Subcellular distribution/translocation of HSP27

As a consequence of the enhanced phosphorylation of HSP27, we aimed to clarify whether Xe-PC induces the translocation of this enzyme. After tissue fractionation, in the cytosolic fraction, there was a slight decrease of HSP27 after xenon administration detectable (Figure 4b, white histogram). Xenon (2.3 ± 0.4 vs 0.8 ± 0.2 in controls, $P < 0.05$) increased the amount of HSP27 in the particulate fraction significantly compared to controls. For isoflurane we could only detect a slight increase of HSP27 in the particulate fraction, which was not statistically significant (1.3 ± 0.3 $P > 0.05$ vs controls, Figure 4b, gray histogram). Uniformity of protein distribution on the respective Western blot was confirmed by detection of α-tubulin. The translocation to the particulate fraction could be blocked by the p38 MAPK inhibitor SB203580 (0.7 ± 0.2, $P < 0.05$ vs Xe-PC, Figure 4b, gray histogram). SB203580 alone had no effect on HSP27 translocation to particulate fractions (0.9 ± 0.4, $P > 0.05$ vs controls).

F-actin fiber formation and colocalization of actin with pHSP27

By immunofluorescence staining of F-actin with rhodamine phalloidin, we could detect an increased polymerization of

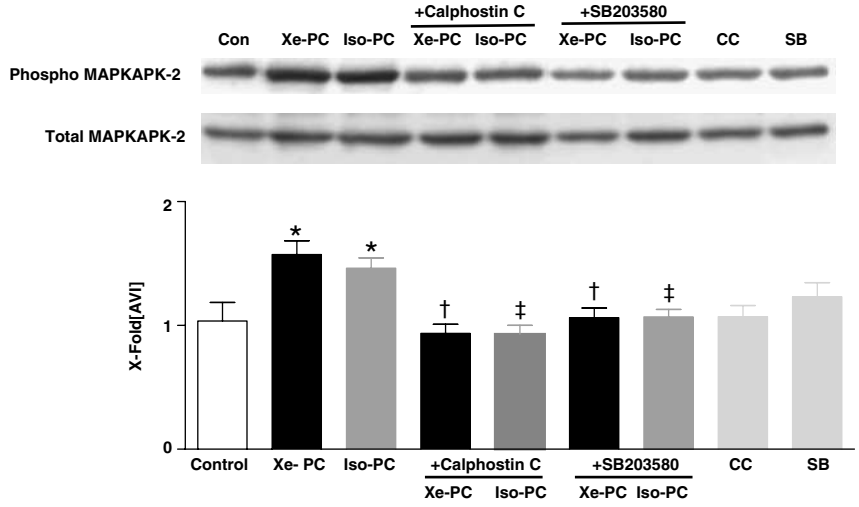

Figure 3 Phosphorylation of MAPKAPK-2 in anesthetic preconditioning. One representative Western blot experiment of cytosolic fraction of control and xenon- or isoflurane-treated hearts in the presence or absence of Calphostin C and SB203580 (each $n = 6$) is shown. Upper panel shows phosphorylated form of MAPKAPK-2, and lower panel total MAPKAPK-2. The histogram presents densitometric evaluation as x-fold average light intensity (AVI). Data show ratio of phosphorylated vs total MAPKAPK-2 (means ± s.e.m.). $^{*}P < 0.05$ vs control, $^{\dagger}P < 0.05$ vs Xe-PC and $^{\ddagger}P < 0.05$ vs Iso-PC.

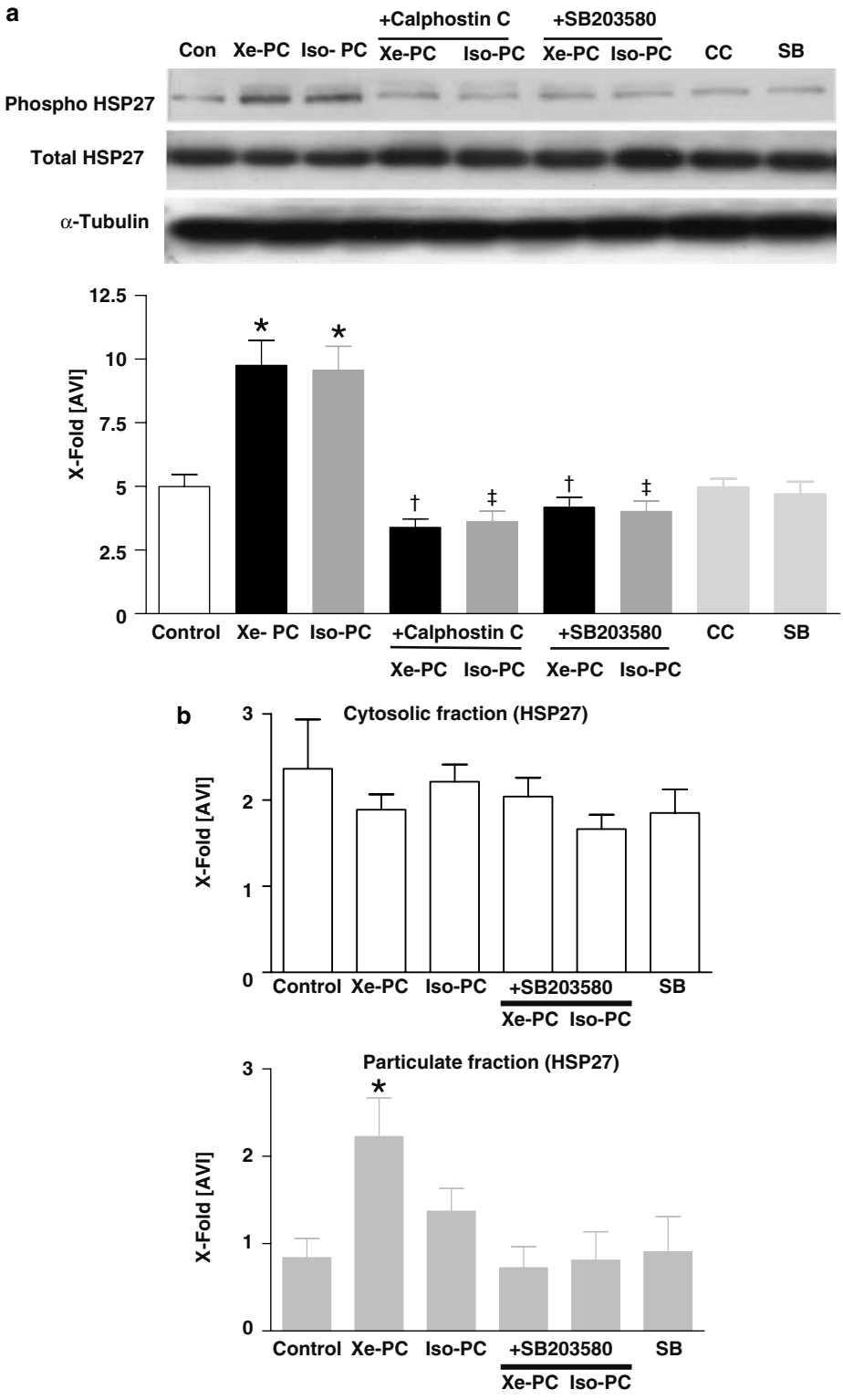

Figure 4 (a) Phosphorylation of HSP27 downstream of p38 MAPK in anesthetic preconditioning. One representative Western blot experiment of cytosolic fraction of control and xenon- or isoflurane-treated hearts in the presence or absence of Calphostin C and SB203580 (each $n=6$) is shown. Upper panel shows phosphorylated form of HSP27, middle panel total HSP27 and lower panel α-tubulin distribution. The histogram presents densitometric evaluation as *x*-fold average light intensity (AVI). Data show ratio of phosphorylated vs total HSP27 (means ± s.e.m.). $^{*}P<0.05$ vs control, $^{\dagger}P<0.05$ vs Xe-PC and $^{\ddagger}P<0.05$ vs Iso-PC. (b) Subcellular distribution/translocation of HSP27. Cytosolic (left panel, white) and particulate (right panel, gray) fraction of control, xenon- and isoflurane-treated hearts in the presence or absence of SB203580 (each $n=6$) was immunoblotted using antibodies against HSP27. α-Tubulin was used in order to test for uniform protein distribution on the blot. The histogram presents densitometric evaluation of all Western blots as *x*-fold average light intensity (AVI). Data show ratio of HSP27 to α-tubulin (means ± s.e.m.). $^{*}P<0.05$ vs control.

actin fibers in xenon- and isoflurane-preconditioned hearts (Figure 5A (b,c)).

To determine if the xenon-induced increase in F-actin fiber formation is associated with a colocalization of actin filaments with pHSP27, we performed costaining of F-actin and phosphorylated HSP27 (Figure 5A (d–f)). As shown by Figure 5A (e, f) both xenon and isoflurane led to an increase of phosphorylated HSP27 (green fluorescence) in the same regions of the myocardial cell, where F-actin fiber formation occurs (red fluorescence). The overlay of both fluorescence stainings shows that phosphorylated HSP27 is colocated with F-actin fibers in all samples (Figure 5A (g–i), yellow fluorescence). However, in xenon- and isoflurane-treated hearts, the colocalization was more pronounced in comparison to the controls (Figure 5A (g–i), yellow fluorescence).

Colocalization of actin with pHSP27 after coimmunoprecipitation in Western blot

The findings from immunofluorescence stainings were confirmed by the use of a coimmunoprecipitation technique with protein-G-agarose. This method allows to coimmunoprecipitate two proteins that form protein/protein interactions from an existing cellular lysate. As demonstrated by Figure 5b, more phosphorylated HSP27 could be detected in the immunoprecipitated lysate of actin after xenon and isoflurane treatment compared with controls. The densitometric evaluation confirms these results as the ratio of pHSP27 per actin in the respective animals is significantly higher after xenon and isoflurane treatment (3.22 ± 0.2 in controls vs 5.7 ± 0.9 after xenon and 5.4 ± 0.4 after isoflurane treatment, both $P < 0.05$). These findings clearly indicate that pHSP27 forms a complex with actin after xenon or isoflurane exposure confirming the data from the immunofluorescence staining.

Discussion

There exists evidence from experimental studies revealing that the 'chemically' inert gas xenon may exert biological 'side effects', which could mediate organ protection. For example, xenon reduced infarct size after regional ischemia when administered during early reperfusion (Preckel *et al*., 2000). In addition, xenon elicits only minimal hemodynamic and cardiovascular side effects (Lachmann *et al*., 1990; Preckel *et al*., 2002b). Taken together this anesthetic gas might be a therapeutic option for patients at high risk for cardiac ischemia or with severely compromised myocardial function.

In this context we could previously show that this anesthetic gas xenon in fact can reduce the infarct size *in vivo* in a *preconditioning* manner when given before the infarct inducing ischemia (Weber *et al*., 2005). Moreover, by the pharmacological blockade of PKC and p38 MAPK pathways we could demonstrate a functional role for both enzymes and that p38 MAPK is located downstream of PKC in xenon-induced cardioprotection (Weber *et al*., 2005).

To date, the final end-effector that mediates the cardioprotection induced by anesthetic preconditioning remains to be elucidated.

Based on these facts, the present study aimed to clarify which other molecular downstream targets of the PKC/p38 MAPK pathway are involved in Xe-PC in comparison to the volatile anesthetic isoflurane. We basically focused on two important targets of p38 MAPK, the MAPKAPK-2 and its downstream target HSP27, since both enzymes play a key role in the reorganization of the cytoskeleton, and, moreover, have been described to be involved in IPC mechanisms of the heart (Sakamoto *et al*., 2000). P38 MAPK is rapidly activated in the heart by diverse stimuli (Clerk *et al*., 1998; Haq *et al*., 1998; Magne *et al*., 2001) and most importantly it plays a role in ischemia reperfusion injury (Abe *et al*., 2000). Following p38 MAPK phosphorylation, the MAPKAPK-2/HSP27 pathway is switched on (Gaestel *et al*., 1991), resulting in the translocation of HSP27 to cytoskeleton constituents of the cell.

The main finding of this study is that xenon administration (70%) directly activates phosphorylation of HSP27 and the MAPKAPK-2 and that this occurs downstream of PKC and p38 MAPK in the signalling cascade. Moreover, we could show that xenon treatment induces not only phosphorylation but also translocation of HSP27 to the particulate fraction of the cell. This translocation was associated with a colocalization of HSP27 to F-actin fibers as shown by immunofluorescence staining and coimmunoprecipitation of the actin/HSP27 complex.

The interpretation of data dealing with changes on the cytoskeleton always depends on the time (i.e. before or after ischemia) when actin polymerization occurs and on the basal status of the cell. In our study the changes in actin polymerization were observed after the preconditioning protocol *before* the heart is subjected to one of the most stressing stimuli: 25 min of ischemia.

Thus, we suggest that the changes of the cytoskeleton prepare the cardiac myocytes to respond adequately to *this subsequent* stress stimulus. Therefore, the increased phosphorylation of HSP27 and the increased F-actin polymerization are a kind of cell preconditioning before the ischemic insult.

The growth of F-actin filaments is determined by factors *that regulate the breakdown of the filament by depolymerization*. According to the polarity of F-actin filament ends, they can bind to several different modulating proteins. Thus, HSP27 as an actin binding protein determines the superstructure of actin filaments and regulates the response of the cell to a certain stimulus.

F-actin fibers additionally contain filamin, topomyosin and myosin in periodical order. Due to their association with myosin they provide contractile properties (Sanger *et al*., 1980) and a dynamic, flexible structure. They prepare the cell to respond appropriatly to different stimuli by cell movement, cell division and changes in cell shape.

Taken together it is not clearly defined whether an increased or inhibited polymerization is protective for the cell. This strongly depends on the stimulus and most importantly on the time when polymerization occurs.

So far, a role for the p38 MAPK/HSP27 pathway in preconditioning phenomena has only been described for IPC (Sakamoto *et al*., 2000), but not for anesthetic-induced preconditioning. Interestingly, the group of Sakamoto *et al*. (2000) also found a direct relationship between PKC and the p38 MAPK/HSP27 pathway. As activation of PKC is one essential step in the signal cascade of anesthetic-induced preconditioning, one might speculate that the p38 MAPK/HSP27 pathway is also involved in anesthetic preconditioning. Moreover, in fact, the present study demonstrates for the first time that the p38 MAPK/HSP27 pathway is involved in

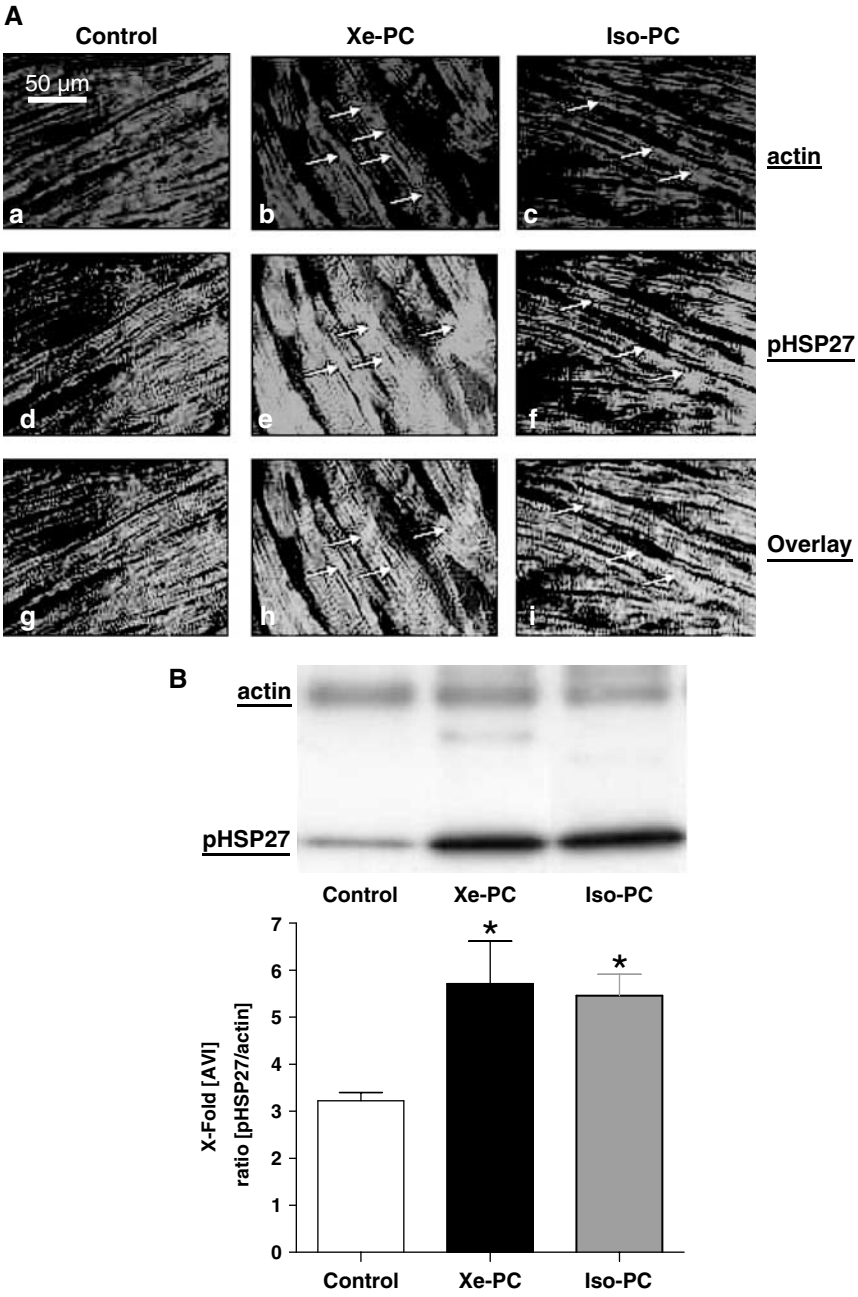

Figure 5 (A) F-actin fiber formation and localization of HSP27. Slides show immunofluorescence-staining experiments. Cryocuts of control (left panels, a/d/g), xenon-treated (middle panels, b/e/h) or isoflurane-treated (right panels, c/f/i) hearts were double stained for F-actin and phosphorylated HSP27. Xenon and isoflurane markedly increased the polymerization of F-actin fibers and this was accompanied by an increased colocalization of HSP27 with F-actin fibers. Stained sections are visualized using a fluorescence microscope with 630-fold magnification (Rhodamine phalloidin: excitation: 554 nm; emission: 573 nm, and Alexa Fluor®: excitation: 497 nm; emission: 519 nm). (B) Coimmunoprecipitation of actin and HSP27 in the particulate fraction. One representative Western blot experiment of immunoprecipitated actin (upper lane) respective pHSP27 (lower lane) of control and xenon- or isoflurane-treated hearts (each $n=6$) is shown. The Western blots were probed for actin and pHSP27 after actin immunoprecipitation from the particulate fraction with protein-G-agarose. The histogram presents densitometric evaluation of all Western blots as *x*-fold average light intensity (AVI) of the ratio of pHSP27 to actin protein. $^*P<0.05$ vs control. (See online for colour figure.)

Xe-PC. To date, there exist only few studies investigating the direct myocardial effects of xenon on a cellular level. The group of Stowe *et al.* (2000) demonstrated that xenon in concentrations up to 80 vol% does not affect the cardiac action potential in isolated guinea-pig hearts and myocytes. Fassl *et al.* (2003) found no effect of xenon on Ca^{2+} currents through L-type Ca^{2+} channels in human atrial cardiomyocytes.

In contrast to this sparse data about xenon actions on the myocardium, there exist more investigations in other cell types. For example, xenon inhibits Ca^{2+}-regulated transitions in the cell cycle of endothelial cells (Petzelt *et al.*, 1999b) and xenon

induces metaphase arrest in rat astrocytes (Petzelt *et al*., 1999a). Two recently published studies by de Rossi *et al*. (2004a, b) investigated the influence of the noble gas on neutrophil adhesion and monocytes *in vitro*. They demonstrated that xenon modulates the expression of adhesion molecules and differentially regulates the LPS-induced NF-κB activation (de Rossi *et al*., 2004a, b).

Nevertheless, so far nothing is known about a potential link between xenon or volatile anesthetic-induced cardioprotection and the cytoskeleton of the myocardial cell. Thus, the results of the present study substantially extend the knowledge about myocardial effects of xenon and the volatile anesthetic isoflurane.

Pharmacological preconditioning induced by *volatile* anesthetics has been investigated in different animal species and in human myocardium *in vitro* and *in vivo* (Cason *et al*., 1997; Novalija *et al*., 1999; Roscoe *et al*., 2000), but as for xenon, the end-effector of isoflurane-induced cardioprotection is not yet known. In our study, isoflurane affected both downstream targets of p38 MAPK, the MAPKAPK-2 and HSP27, to a similar extent as xenon. However, isoflurane failed to induce translocation of HSP27 to the particulate fraction, suggesting that in part the molecular pathways differ between xenon- and isoflurane-mediated *pharmacological preconditioning*.

A relationship between isoflurane-induced early preconditioning and p38MAPK/HSP27 pathways has not yet been described in the heart. Since the role of p38 MAPK pathways in anesthetic-induced preconditioning is yet a matter of controversy, we aimed to further confirm our previous findings of an increased phosphorylation of p38 MAPK by the use of an enzyme *activity* measurement. In fact, both anesthetics increased ATF-2 phosphorylation, a direct substrate of p38 MAPK, demonstrating that the activity of this MAPK is affected by xenon and isoflurane. Similar to our results, a very recently published study by Zheng and co-workers showed that the p38 MAPK pathway is involved in isoflurane-induced late preconditioning of the rat brain (Zheng & Zuo, 2004). In contrast, Da Silva *et al*. (2004) found no role for p38 MAPK in isoflurane-induced preconditioning, using 1.5 MAC isoflurane in the isolated rat heart. However, this study also investigated the well-described IPC and revealed that in IPC, p38 MAPK and also HSP27 play a key role (Da Silva *et al*., 2004). They documented an accumulation of HSP27 to myofibrillar structures of the cell in response to ischemic but not anesthetic preconditioning (Da Silva *et al*., 2004). A very recent study of Sergeev *et al*. (2004) compared the trigger-dependent gene expression profiles of ischemic- and anesthetic-induced cardioprotection. They found a strong upregulation for HSP27 and HSP70 only in IPC and not after 2 h of 1.5 MAC isoflurane administration (Sergeev *et al*., 2004). This study had an important limitation not allowing a direct comparison with our study. In the experimental protocol, there was no washout of the anesthetic agent, suggesting rather a *treatment* than a *preconditioning* effect of isoflurane (Sergeev *et al*., 2004).

In addition, these divergent data may be explained by the use of different doses of anesthetics and especially by the distinct discrepancy between *in vivo* and *in vitro* situations.

Interestingly, already in 1999, Ismaeil and co-workers showed that an intact cytoskeleton is critically important in isoflurane-induced preconditioning (Ismaeil *et al*., 1999). They used the microtubule depolymerizing agent Colchicine in an *in vivo* rabbit model and demonstrated that the infarct size reduction exerted by the volatile anesthetic isoflurane was abolished (Ismaeil *et al*., 1999). These results strongly support our data and suggest that the cytoskeleton is critically involved in cardioprotective effects of anesthetic-induced preconditioning.

However, only the functional blockade of one of the investigated enzymes *in vivo* (pharmacological blockade or knock out animals) followed by infarct size measurement would give the final proof of the implication of this pathway. Unfortunately, to our knowledge, there exist no MAPKAPK-2 or HSP27 blockers that can be used *in vivo*. Most of the inhibitors have only been extensively used *in vitro*. Therefore, it is currently not possible to block the respective enzyme in the rat *in vivo* and to measure a functional parameter. Thus, we have to conclude that from the fact that the blockade of the main upstream enzyme of MAPKAPK-2 and HSP27, the p38 MAPK, results in a complete loss of cardioprotection; it is supposable that the cytoskeleton pathway is implicated in the Xe-PC signalling cascade.

Regarding the definition of preconditioning, it should be mentioned that the cardioprotective stimulus (e.g. xenon) should no more be present during ischemia. This was achieved in our experiments by a high fresh gas flow during the washout period in order to permit a sufficient wash out of xenon and isoflurane. Moreover, the noble gas xenon has an extremely low blood : gas partition coefficient and shows an extremely rapid onset and offset of its action.

A potential limitation of our study is the fact that the pharmacological inhibitors like Calphostin C and SB203580 may affect other enzymes to a certain extent. Their specificity strongly depends on the concentration used. For example, Calphostin C inhibits PKC with an IC_{50} of 50 nM, and other kinases like PKA ($IC_{50} > 50\,\mu$M), $p60^{v\text{-}src}$ ($IC_{50} > 50\,\mu$M) and PKG ($IC_{50} > 25\,\mu$M) are inhibited only at higher concentrations. The second inhibitor, SB203580, inhibits other kinases only when used in concentrations higher than 10 μM (Davies *et al*., 2000). Based on these facts we used a comparably low dose of both inhibitors administered by a bolus injection ($0.1\,mg\,kg^{-1}$ (12 μM) Calphostin C and $1\,mg\,kg^{-1}$ (2.4 μM) SB203580) in accordance with other *in vivo* studies of the literature (Li & Kloner, 1995; Fryer *et al*., 2001).

We used only one equipotent concentration of xenon or isoflurane, and our results must be limited to this concentration. However, not the anesthetic properties of xenon and isoflurane, but their cardioprotective effects were the main subject of the present study.

In summary, the present study provides new insights into the underlying molecular mechanisms of xenon- and isoflurane-induced myocardial protection by pharmacological preconditioning. This cardioprotection is linked to the p38 MAPK/HSP27 pathway and involves a reorganization of the myocardial cytoskeleton by the noble gas. In our study, the volatile anesthetic isoflurane did not induce the translocation of HSP27 *in the used dose* to a significant extent. However, there is a tendency of an increased HSP27 translocation after isoflurane treatment. Together with our previous results, which showed that p38 MAPK blockade *in vivo* abolishes cardioprotection (Weber *et al*., 2005), the p38 MAPK/HSP27 pathway is suggested to be the potential mediator of anesthetic-induced preconditioning as p38 MAPK is the main upstream target of MAPKAK-2 and HSP27.

Of course, the data presented here are limited to the experimental animal model and it is not possible to transfer the results to the clinical situation. Nevertheless, understanding the molecular mechanisms of the cardioprotection exerted by xenon as an anesthetic *gas* may help to expand knowledge on xenon as a potential ideal anesthetic gas for patients with a high-risk for cardiac events.

This study was supported by a grant from the Else Kröner-Fresenius Stiftung, Bad Homburg, Germany, and by a grant from the European Society of Anaesthesiology (ESA). Xenon was generously supplied by Messer Griesheim GmbH, Vertrieb Medical, 47805 Krefeld, Germany. The excellent technical support of Claudia Dohle and Yvonne Grüber is gratefully acknowledged. O. Toma was supported by the Catholic Academic Exchange service (KAAD).

References

ABE, J., BAINES, C.P. & BERK, B.C. (2000). Role of mitogen-activated protein kinases in ischemia and reperfusion injury: the good and the bad. *Circ. Res.,* **86,** 607–609.

BENNDORF, R., HAYESS, K., RYAZANTSEV, S., WIESKE, M., BEHLKE, J. & LUTSCH, G. (1994). Phosphorylation and supramolecular organization of murine small heat shock protein HSP25 abolish its actin polymerization-inhibiting activity. *J. Biol. Chem.,* **269,** 20780–20784.

BITAR, K.N. (2002). HSP27 phosphorylation and interaction with actin-myosin in smooth muscle contraction. *Am. J. Physiol. Gastrointest. Liver Physiol.,* **282,** G894–G903.

CASON, B.A., GAMPERL, A.K., SLOCUM, R.E. & HICKEY, R.F. (1997). Anesthetic-induced preconditioning: previous administration of isoflurane decreases myocardial infarct size in rabbits. *Anesthesiology,* **87,** 1182–1190.

CHEN, Y., RAJASHREE, R., LIU, Q. & HOFMANN, P. (2003). Acute p38 MAPK activation decreases force development in ventricular myocytes. *Am. J. Physiol. Heart Circ. Physiol.,* **285,** H2578–H2586.

CLERK, A., MICHAEL, A. & SUGDEN, P.H. (1998). Stimulation of multiple mitogen-activated protein kinase sub-families by oxidative stress and phosphorylation of the small heat shock protein, HSP25/27, in neonatal ventricular myocytes. *Biochem. J.,* **333** (Part 3), 581–589.

DA SILVA, R., GRAMPP, T., PASCH, T., SCHAUB, M.C. & ZAUGG, M. (2004). Differential activation of mitogen-activated protein kinases in ischemic and anesthetic preconditioning. *Anesthesiology,* **100,** 59–69.

DAVIES, S.P., REDDY, H., CAIVANO, M. & COHEN, P. (2000). Specificity and mechanism of action of some commonly used protein kinase inhibitors. *Biochem. J.,* **351,** 95–105.

DE ROSSI, L.W., BRUECKMANN, M., REX, S., BARDERSCHNEIDER, M., BUHRE, W. & ROSSAINT, R. (2004a). Xenon and isoflurane differentially modulate lipopolysaccharide-induced activation of the nuclear transcription factor KB and production of tumor necrosis factor-alpha and interleukin-6 in monocytes. *Anesth. Analg.,* **98,** 1007–1012.

DE ROSSI, L.W., HORN, N.A., STEVANOVIC, A., BUHRE, W., HUTSCHENREUTER, G. & ROSSAINT, R. (2004b). Xenon modulates neutrophil adhesion molecule expression *in vitro*. *Eur. J. Anaesthesiol.,* **21,** 139–143.

FASSL, J., HALASZOVICH, C.R., HUNEKE, R., JUNGLING, E., ROSSAINT, R. & LUCKHOFF, A. (2003). Effects of inhalational anesthetics on L-type Ca2+ currents in human atrial cardiomyocytes during beta-adrenergic stimulation. *Anesthesiology,* **99,** 90–96.

FRYER, R.M., HSU, A.K. & GROSS, G.J. (2001). ERK and p38 MAP kinase activation are components of opioid-induced delayed cardioprotection. *Basic Res. Cardiol.,* **96,** 136–142.

GAESTEL, M., SCHRODER, W., BENNDORF, R., LIPPMANN, C., BUCHNER, K., HUCHO, F., ERDMANN, V.A. & BIELKA, H. (1991). Identification of the phosphorylation sites of the murine small heat shock protein hsp25. *J. Biol. Chem.,* **266,** 14721–14724.

GUAY, J., LAMBERT, H., GINGRAS-BRETON, G., LAVOIE, J.N., HUOT, J. & LANDRY, J. (1997). Regulation of actin filament dynamics by p38 MAP kinase-mediated phosphorylation of heat shock protein 27. *J. Cell Sci.,* **110,** 357–368.

HAQ, S.E., CLERK, A. & SUGDEN, P.H. (1998). Activation of mitogen-activated protein kinases (p38-MAPKs, SAPKs/JNKs and ERKs) by adenosine in the perfused rat heart. *FEBS Lett.,* **434,** 305–308.

ISMAEIL, M.S., TKACHENKO, I., HICKEY, R.F. & CASON, B.A. (1999). Colchicine inhibits isoflurane-induced preconditioning. *Anesthesiology,* **91,** 1816–1822.

KANG, N., ALEXANDER, G., PARK, J.K., MAASCH, C., BUCHWALOW, I., LUFT, F.C. & HALLER, H. (1999). Differential expression of protein kinase C isoforms in streptozotocin-induced diabetic rats. *Kidney Int.,* **56,** 1737–1750.

LACHMANN, B., ARMBRUSTER, S., SCHAIRER, W., LANDSTRA, M., TROUWBORST, A., VAN DAAL, G.J., KUSUMA, A. & ERDMANN, W. (1990). Safety and efficacy of xenon in routine use as an inhalational anaesthetic. *Lancet,* **335,** 1413–1415.

LI, Y. & KLONER, R.A. (1995). Does protein kinase C play a role in ischemic preconditioning in rat hearts? *Am. J. Physiol.,* **268,** H426–H431.

LOWRY, O.H., ROSEBROUGH, N.J., FARR, A.L. & RANDALL, R.J. (1951). Protein measurement with the folin phenol reagent. *J. Biol. Chem.,* **193,** 265–275.

MACKAY, K. & MOCHLY-ROSEN, D. (2001). Arachidonic acid protects neonatal rat cardiac myocytes from ischaemic injury through epsilon protein kinase C. *Cardiovasc. Res.,* **50,** 65–74.

MAGNE, S., COUCHIE, D., PECKER, F. & PAVOINE, C. (2001). Beta(2)-adrenergic receptor agonists increase intracellular free Ca(2+) concentration cycling in ventricular cardiomyocytes through p38 and p42/44 MAPK-mediated cytosolic phospholipase A(2) activation. *J. Biol. Chem.,* **276,** 39539–39548.

MIRON, T., VANCOMPERNOLLE, K., VANDEKERCKHOVE, J., WILCHEK, M. & GEIGER, B. (1991). A 25-kD inhibitor of actin polymerization is a low molecular mass heat shock protein. *J. Cell Biol.,* **114,** 255–261.

MULLENHEIM, J., EBEL, D., BAUER, M., OTTO, F., HEINEN, A., FRASSDORF, J., PRECKEL, B. & SCHLACK, W. (2003). Sevoflurane confers additional cardioprotection after ischemic late preconditioning in rabbits. *Anesthesiology,* **99,** 624–631.

MULLENHEIM, J., EBEL, D., FRASSDORF, J., PRECKEL, B., THAMER, V. & SCHLACK, W. (2002). Isoflurane preconditions myocardium against infarction *via* release of free radicals. *Anesthesiology,* **96,** 934–940.

MULLENHEIM, J., FRASSDORF, J., PRECKEL, B., THAMER, V. & SCHLACK, W. (2001). Ketamine, but not S(+)-ketamine, blocks ischemic preconditioning in rabbit hearts *in vivo*. *Anesthesiology,* **94,** 630–636.

NOVALIJA, E., FUJITA, S., KAMPINE, J.P. & STOWE, D.F. (1999). Sevoflurane mimics ischemic preconditioning effects on coronary flow and nitric oxide release in isolated hearts. *Anesthesiology,* **91,** 701–712.

PETZELT, C., TASCHENBERGER, G., SCHMEHL, W., HAFNER, M. & KOX, W.J. (1999a). Xenon induces metaphase arrest in rat astrocytes. *Life Sci.,* **65,** 901–913.

PETZELT, C., TASCHENBERGER, G., SCHMEHL, W. & KOX, W.J. (1999b). Xenon-induced inhibition of Ca2+-regulated transitions in the cell cycle of human endothelial cells. *Pflugers Arch.,* **437,** 737–744.

PRECKEL, B., EBEL, D., MULLENHEIM, J., FRASSDORF, J., THAMER, V. & SCHLACK, W. (2002a). The direct myocardial effects of xenon in the dog heart *in vivo*. *Anesth. Analg.,* **94,** 545–551.

PRECKEL, B., MULLENHEIM, J., MOLOSCHAVIJ, A., THAMER, V. & SCHLACK, W. (2000). Xenon administration during early reperfusion reduces infarct size after regional ischemia in the rabbit heart *in vivo*. *Anesth. Analg.,* **91,** 1327–1332.

PRECKEL, B., SCHLACK, W., HEIBEL, T. & RUTTEN, H. (2002b). Xenon produces minimal haemodynamic effects in rabbits with chronically compromised left ventricular function. *Br. J. Anaesth.,* **88,** 264–269.

RAMPIL, I.J., LASTER, M.J. & EGER, E.I. (2001). Antagonism of the 5-HT(3) receptor does not alter isoflurane MAC in rats. *Anesthesiology,* **95,** 562–564.

ROSCOE, A.K., CHRISTENSEN J.D & LYNCH III, C. (2000). Isoflurane, but not halothane, induces protection of human myocardium *via* adenosine A1 receptors and adenosine triphosphate-sensitive potassium channels. *Anesthesiology,* **92,** 1692–1701.

ROSSAINT, R., REYLE-HAHN, M., SCHULTE AM, E.J., SCHOLZ, J., SCHERPEREEL, P., VALLET, B., GIUNTA, F., DEL TURCO, M., ERDMANN, W., TENBRINCK, R., HAMMERLE, A.F. & NAGELE, P. (2003). Multicenter randomized comparison of the efficacy and safety of xenon and isoflurane in patients undergoing elective surgery. *Anesthesiology,* **98,** 6–13.

SAKAMOTO, K., URUSHIDANI, T. & NAGAO, T. (2000). Translocation of HSP27 to sarcomere induced by ischemic preconditioning in isolated rat hearts. *Biochem. Biophys. Res. Commun.,* **269,** 137–142.

SANGER, J.W., SANGER, J.M., KREIS, T.E. & JOCKUSCH, B.M. (1980). Reversible translocation of cytoplasmic actin into the nucleus caused by dimethyl sulfoxide. *Proc. Natl. Acad. Sci. U.S.A.,* **77,** 5268–5272.

SCHMIDT, M., MARX, T., KOTZERKE, J., LUDERWALD, S., ARMBRUSTER, S., TOPALIDIS, P., SCHIRMER, U. & REINELT, H. (2001). Cerebral and regional organ perfusion in pigs during xenon anaesthesia. *Anaesthesia,* **56,** 1154–1159.

SERGEEV, P., DA SILVA, R., LUCCHINETTI, E., ZAUGG, K., PASCH, T., SCHAUB, M.C. & ZAUGG, M. (2004). Trigger-dependent gene expression profiles in cardiac preconditioning: evidence for distinct genetic programs in ischemic and anesthetic preconditioning. *Anesthesiology,* **100,** 474–488.

STOWE, D.F., REHMERT, G.C., KWOK, W.M., WEIGT, H.U., GEORGIEFF, M. & BOSNJAK, Z.J. (2000). Xenon does not alter cardiac function or major cation currents in isolated guinea pig hearts or myocytes. *Anesthesiology,* **92,** 516–522.

WEBER, N.C., TOMA, O., WOLTER, J.I., OBAL, D., MÜLLENHEIM, J., PRECKEL, B. & SCHLACK, W. (2005). The noble gas Xenon induces pharmacological preconditioning in the rat heart *in vivo via* induction of PKC-epsilon and p38 MAPK. *Br. J. Pharmacol.,* **144,** 123–132.

ZHENG, S. & ZUO, Z. (2004). Isoflurane preconditioning induces neuroprotection against ischemia *via* activation of P38 mitogen-activated protein kinases. *Mol. Pharmacol.,* **65,** 1172–1180.

(Received January 31, 2005
Revised May 3, 2005
Accepted June 1, 2005
Published online 8 August 2005)